bioRxiv preprint doi: https://doi.org/10.1101/2022.09.30.510364; this version posted October 1, 2022. The copyright holder for this preprint (which was not certified by peer review) is the author/funder, who has granted bioRxiv a license to display the preprint in perpetuity. It is made available under aCC-BY-NC-ND 4.0 International license.

Actin cytoskeleton dynamics affect replication of Human Metapneumovirus

Pamela Elizabeth Rodríguez[1§], Pedro Ignacio Gil[2§], Jorge Augusto Cámara[1], Alicia Cámara[1] and María Gabriela Paglini*[2,3]

[1]Laboratory of Influenza and other Respiratory Viruses, Virology Institute "Dr. J. M. Vanella". Facultad de Ciencias Médicas. Universidad Nacional de Córdoba. Córdoba. Córdoba. Argentina.
[2]Laboratory of Cell Biology of Viral Infection, Virology Institute "Dr. J. M. Vanella". Facultad de Ciencias Médicas. Universidad Nacional de Córdoba. Córdoba. Córdoba. Argentina.
[3]Laboratory of Neurophysiology, Instituto de Investigación Médica Mercedes y Martín Ferreyra, INIMEC-CONICET, Universidad Nacional de Córdoba, Córdoba, Argentina.

§: Both authors contributed equally to this work.

***Corresponding author.**
María Gabriela Paglini, Ph.D.
Laboratory of Cell Biology of Viral Infection, Virology Institute "Dr. J. M. Vanella". Facultad de Ciencias Médicas. Universidad Nacional de Córdoba. Córdoba. Argentina,
Enfermera Gordillo s/n. Ciudad Universitaria, 5000 - Córdoba Argentina.
Phone: +54-351-4334022
E-mail: gpaglini@immf.uncor.edu

Running title.

Human Metapneumovirus replication dynamics

Keywords.

Virus biology; Replication cycle; Actin filaments; Cytochalasin D; Respiratory disease.

bioRxiv preprint doi: https://doi.org/10.1101/2022.09.30.510364; this version posted October 1, 2022. The copyright holder for this preprint (which was not certified by peer review) is the author/funder, who has granted bioRxiv a license to display the preprint in perpetuity. It is made available under aCC-BY-NC-ND 4.0 International license.

ABSTRACT

Human metapneumovirus (hMPV) is a virus responsible for acute respiratory infection in humans with clinical and epidemiological relevance in pediatric, immunocompromised, and elderly populations. Little is known about hMPV *in vitro* replication biological processes and their relationship with cellular structures such as the cytoskeleton. Our goal was to evaluate the viral replication curve in order to study the role of the actin cytoskeleton in hMPV replication at different stages of viral growth. Human metapneumovirus was isolated in a Vero cell line from a clinical sample and identified as A_2 genotype. The cytopathic effect was detected by the appearance of cell rounding and refractory cell clusters. The growth curve showed that viral replication maximum level was between 48 and 72 h.p.i. The highest percentage of infected cells and intracellular hMPV-protein were detected at the early stages of the replication cycle (8 h.p.i). Disruption of actin microfilaments with cytochalasin D (CytD) during the early events of infection provoked an increase in both intracellular and extracellular viruses. We demonstrate that the early phase of the hMPV curve is crucial for viral replication. We also show that disruption of actin filaments during this time increments both viral protein expression in the cytoplasm and the release of viruses to the extracellular space. This study contributes to elucidate wild-type hMPV growth kinetics, providing new insights on the actin cytoskeleton role in viral replication mechanisms. In addition, it points out putative targets to develop new antiviral treatments.

bioRxiv preprint doi: https://doi.org/10.1101/2022.09.30.510364; this version posted October 1, 2022. The copyright holder for this preprint (which was not certified by peer review) is the author/funder, who has granted bioRxiv a license to display the preprint in perpetuity. It is made available under aCC-BY-NC-ND 4.0 International license.

INTRODUCTION

Human Metapneumovirus (hMPV) and Respiratory syncytial virus (RSV) cause severe respiratory diseases in infants and elderly adults (Shafagati and Williams, 2018). Both viruses belong to the *Pneumoviridae* family (Afonso et al., 2016) and no vaccine or approved antiviral therapy currently exists for hMPV. Besides, there is only one prophylactic treatment to control RSV (Kinder et al., 2020). Human Metapneumovirus is an enveloped negative-stranded RNA virus with a non-segmented genome composed of eight genes encoding for nine proteins (Ballegeer and Saelens, 2020). Two major hMPV subtypes have been described: A (A1, A2a, A2b1, A2b2) and B (B1, B2) (Afonso et al., 2016; Nao et al., 2020; Shafagati and Williams, 2018; Van Den Hoogen et al., 2001).

Since the discovery of hMPV (Van Den Hoogen et al., 2001), several approaches for its *in vitro* isolation have been followed. Viral adaptation and spread in cell cultures are difficult since both require high viral loads and successive blind passages of about 14 to 21 days to visualize the cytopathic effect (CPE), characterized by changes in cell morphology or by the formation of syncytia (Boivin et al., 2002; Chan et al., 2003; Deffrasnes et al., 2005; Jumat et al., 2014; Sato et al., 2017).

The viral infection cycle begins with the entry of viral particles into susceptible cells through the interaction with receptors that trigger the internalization process. Several studies have reported an important role for the cytoskeleton, particularly actin microfilaments (MFLs), in the entry and replication of numerous viruses, including hMPV, into the host cell (Cifuentes-Muñoz et al., 2020; Merwaiss et al., 2018; Najjar et al., 2016; Roberts et al., 2015). In this sense, it has been shown that actin cytoskeleton components are essential cofactors for RSV replication, spread, and morphogenesis (Kallewaard et al., 2005; Mehedi et al., 2016; Shahriari et al., 2016; Shahriari et al., 2018). Moreover, previous studies from our laboratory demonstrated that the disruption of the actin cytoskeleton during the early stage of Pixuna

bioRxiv preprint doi: https://doi.org/10.1101/2022.09.30.510364; this version posted October 1, 2022. The copyright holder for this preprint (which was not certified by peer review) is the author/funder, who has granted bioRxiv a license to display the preprint in perpetuity. It is made available under aCC-BY-NC-ND 4.0 International license.

74 virus (PIXV) replication, increased the extracellular viral yields, probably promoting
75 endocytosis and thus increasing the entry of viral particles (Gil et al., 2017).

76 Despite the importance of hMPV as an etiological agent of human respiratory pathologies, the
77 mechanisms of interaction between the virus and the host cell to secure infection remain
78 largely unexplored. In the present study, we examined the role of the actin cytoskeleton in
79 hMPV replication at different stages of viral growth. To this end, we isolated and identified
80 hMPV circulating in Cordoba, Argentina. Furthermore, we describe the hMPV replication
81 curve and characterize the subcellular expression of viral proteins at different times after
82 infection. We demonstrate that actin depolymerization at the early phase of the hMPV
83 replication curve is crucial for a successful viral replication. The presence of cytochalasin D
84 (CytD) during this period increased viral protein expression in the cytoplasm and also the
85 release of viruses to the extracellular space.

86 Considering that hMPV causes a severe disease, identifying the molecular mechanisms
87 underlying its replication cycle broadens our understanding of the cell biology of viral
88 infection. Morever, it provides possible targets to develop new antiviral treatments.

89

90 **RESULTS**

91 **Human Metapneumovirus isolation and identification**

92 Human Metapneumovirus was isolated from nasopharyngeal aspirates of hospitalized young
93 children in Cordoba, Argentina. The isolated virus replicated in cultures of Vero cells in the
94 third passage at 14 d.p.i., after two blind passages of 21 days each one. The viral CPE was
95 characterized by cell rounding, detachment, and formation of refractory cell clusters (Fig.
96 1A). In order to confirm that the CPE was caused by hMPV, immunofluorescence (IF)
97 detection was performed on infected monolayers. The presence of specific hMPV proteins

bioRxiv preprint doi: https://doi.org/10.1101/2022.09.30.510364; this version posted October 1, 2022. The copyright holder for this preprint (which was not certified by peer review) is the author/funder, who has granted bioRxiv a license to display the preprint in perpetuity. It is made available under aCC-BY-NC-ND 4.0 International license.

was observed at 4, 7, and 14 d.p.i. located and distributed in the cell cytoplasm presenting a dotted pattern (Fig. 1B). Simultaneously, virus genome detection by nucleic acid amplification assays (RT-PCR) from supernatants of infected Vero cell cultures collected at 4, 7, and 14 d.p.i. were positive for the amplification of the 199 bp N protein fragment (Fig. 1C), confirming the presence of hMPV in supernatants of infected Vero cells. To typify viral isolation, a maximum likelihood tree was built, based on the amplified region of the gene for the fusion protein (F). The Cordoba/ARG/3864/2015 local isolated strain (access no: MN117139) was identified as A_2 hMPV and grouped with Canada and The Netherlands prototype strains, and with sequences from Argentina (Galiano et al., 2006), Peru, Brazil, United States, China, and Italy (Fig. 1F).

As previously reported, a common feature of *Pneumovirus* and *Paramyxovirus* infection is the formation of punctate areas of concentrated viral proteins called viral inclusion bodies (Cifuentes-muñoz et al., 2017). Thus, different subcellular localization of big fluorescent dots were observed several times after infection (Fig. 1B and D) whereas by confocal microscopy, small dots were detected between 0 and 96 h.p.i. in the subcortical area enriched in actin filaments (Fig. 1E, low panel).

The hMPV replication cycle

In order to describe the hMPV growth curve, extracellular viral production over time was evaluated by qRT-PCR expressed as the number of copies of RNA/µl of culture supernatant. The progressive increase in the number of copies of RNA was observed until 72 h.p.i., with a maximum of 4,961 copies of extracellular viral RNA/µl of supernatant (Fig. 2A, plot right axis). The time course of hMPV infection was also studied by IF. The presence of viral proteins was quantified as the number of fluorescent dots/infected cell (Fig. 2A, plot left axis and C). Interestingly, the number of fluorescent dots/infected cell decreased while the number

bioRxiv preprint doi: https://doi.org/10.1101/2022.09.30.510364; this version posted October 1, 2022. The copyright holder for this preprint (which was not certified by peer review) is the author/funder, who has granted bioRxiv a license to display the preprint in perpetuity. It is made available under aCC-BY-NC-ND 4.0 International license.

of copies of RNA/µl of culture supernatant increased. At 72 h.p.i. the maximum extracellular viral yield corresponded to the minimum number of fluorescent dots in the cytoplasm, as well as to the lowest percentage of infected cells (Fig. 2A and B). It is important to highlight that the percentage of infected cells decreased significantly and progressively from 24 h.p.i. until the end of the experiment (Fig. 2 B and C).

Taken together, our results demonstrate that the highest percentage of infected cells and intracellular hMPV-protein contents were detected at the early phase of the replication cycle. While the cycle progressed, hMPV immunostaining decreased whereas extracellular RNA viral copies increased due to the release of the viral progeny.

Perturbation of actin microfilaments at different stages of the viral cycle affects hMPV replication

Previous studies have reported that the cytoskeleton, particularly the actin microfilaments (MFLs), plays an important role during the entry and replication of numerous viruses into the host cell (Cifuentes-Muñoz et al., 2020). Therefore, we studied the role of MFLs at early and late stages of hMPV infection cycle. For this purpose, disruption of actin polymerization was performed using CytD at different times during hMPV infection cycle. We first determined the participation of MFLs during the entry of the virus into the cell and at its early stages of replication. To this end, CytD was applied during virus infection (2 hours), during the first 8 h.p.i. and during the first 24 h.p.i.

Treatment with CytD during the early stages of the replication cycle prevented the above mentioned significant decrease in the number of infected cells, regardless of whether the drug was applied during infection or during the first 8 or 24 h.p.i., thus maintaining the initial percentage of infected cells (Fig. 3A and B). Interestingly, CytD treatment during the first 24 h.p.i., also prevented the dramatic diminution in the percentage of infected cells at 72 h.p.i.

bioRxiv preprint doi: https://doi.org/10.1101/2022.09.30.510364; this version posted October 1, 2022. The copyright holder for this preprint (which was not certified by peer review) is the author/funder, who has granted bioRxiv a license to display the preprint in perpetuity. It is made available under aCC-BY-NC-ND 4.0 International license.

compared to controls (Fig. 3 B). To obtain a quantitative measure of CytD effect on F viral protein expression at the different stages of the viral replication cycle, we quantified the number of fluorescent dots/infected cell.

Treatment with CytD during infection or during the first 8 h.p.i. caused a significant increase in fluorescent dots per infected cell compared to controls (vehicle). In particular, during the first 8 h of drug treatment a 2 to 2.5 fold increase was observed at both analyzed times (8 and 24 h.p.i.) (Fig. 3 A and C). When CytD was applied during the first 24 h.p.i., and quantified at the end of the treatment, no significant differences in the number of fluorescent dots per infected cells was observed compared to controls, however, incubation with the drug prevented the loss of viral protein detected in control cells at 72 h.p.i. (Fig. 3 C).

Finally, to determine virus yields in the extracellular medium, we quantified the number of viral RNA copies in the culture supernatant (Figure 3 D). CytD treatment during the infection period and during the first 8 h.p.i significantly increased viral production at 24 h.p.i. (see the accumulated value). On the other hand, CytD treatment during the first 24 h.p.i., caused a significant decrease in extracellular RNA viral copies at 24 h.p.i. This reduction in extracellular RNA viral copies remained unchanged up to 72 h.p.i., as can be observed in the accumulated values (Fig. 3 D).

In addition, we focused on the late stage of the replication curve and observed that CytD applied during the last 24 h.p.i (48-72 h.p.i) caused no changes in the percentage of infected cells, in the number of dots/infected cell or in the number of extracellular RNA viral copies compared to vehicle controls (data not shown).

Altogether, these data suggest that the first 8 hours of the hMPV infection curve are crucial for viral replication. Moreover, they show that the presence of CytD during this period results in an increment of viral protein expression in the cell cytoplasm and also in the release of viruses to the extracellular space.

bioRxiv preprint doi: https://doi.org/10.1101/2022.09.30.510364; this version posted October 1, 2022. The copyright holder for this preprint (which was not certified by peer review) is the author/funder, who has granted bioRxiv a license to display the preprint in perpetuity. It is made available under aCC-BY-NC-ND 4.0 International license.

DISCUSSION

In this study we report the first successful isolation of hMPV performed in a Vero-CCL cell line obtained from a positive clinical sample in Cordoba city, Argentina. We identified this local strain and described the viral replication curve showing that the maximum viral production takes place at 72 h.p.i. Moreover, we demonstrate that the disruption of actin MFL at the early stages of infection increases both intra- and extracellular viral production.

The viral isolate was identified as A_2 hMPV subtype by phylogenetic analysis. This result agrees with our previous studies where we have reported circulation of the A_2 hMPV subtype in Argentina (Rodriguez et al., 2020). In addition, co-circulation of this subtype with other genotypes such as A_1, B_1, and B_2 have been previously reported (Galiano et al., 2006; Velez Rueda et al., 2013). Notwithstanding, genotype predominance also depends on factors suchs as epidemiological year and region, host immunity and susceptibility (Choe et al., 2020; Kim et al., 2010; Zhang et al., 2012a; Zhou et al., 2020). The A_2 genotype is clinically relevant because it may cause diseases of varying severity. Moreover, this genotype has been reported to cause very severe conditions as pneumonia and hypoxia, leading to more admissions in intensive care units compared to the other subtypes (Arnott et al., 2013; Vicente et al., 2006).

The isolation of A_2 hMPV viral strain, showed the first signs of CPE in the third blind passage, at 14 d.p.i, characterized by cell rounding and formation of refractive corsages of cells, similarly to what has been previously reported (Abiko et al., 2007; Boivin et al., 2002; Chan et al., 2003; Deffrasnes et al., 2005; Kinder et al., 2020). In contrast, other authors have described that hMPV can appear as a syncytium (Bernal et al., 2019; Sato et al., 2017; Van Den Hoogen et al., 2001; Yang et al., 2016) such as RSV (member of the same family) and this difference in CPE may be related to the cell lines that were infected (e.g. LLC-MK2) or to the viral genotype (Jumat et al., 2014; Nao et al., 2019; Reina et al., 2007; Tollefson et al.,

bioRxiv preprint doi: https://doi.org/10.1101/2022.09.30.510364; this version posted October 1, 2022. The copyright holder for this preprint (which was not certified by peer review) is the author/funder, who has granted bioRxiv a license to display the preprint in perpetuity. It is made available under aCC-BY-NC-ND 4.0 International license.

2010; Williams et al., 2005; Zhang et al., 2012b). It is important to highlight that numerous authors report that hMPV isolation is difficult (Deffrasnes et al., 2005; Jumat et al., 2014; Lee et al., 2019; Loo et al., 2013; Schowalter et al., 2006; Tollefson et al., 2010; Van Den Hoogen et al., 2001). In this sense, it is known that isolation of respiratory viruses from clinical specimens often show low efficiency in *in vitro* cell cultures. This low efficiency could be associated to the cell type and/or the virus subtype and its entry pathway (Cifuentes-muñoz et al., 2017; Cifuentes-Muñoz and Ellis Dutch, 2019; Cox et al., 2015; Kinder et al., 2020; Lee et al., 2019; Yang et al., 2016).

The hMPV strain replication curve showed an exponential phase between 48 to 72 h.p.i., the highest intracellular viral protein concentration was at 8 h.p.i. which is consistent with results obtained by other groups. Tollefson (2010) described hMPV kinetics in LLC-MK2 cells, with the eclipse phase at 24 h.p.i. and the exponential phase between 48 and 72 h.p.i. with a significant increase in viral titer. El Najjar (2016) showed maximum viral production at 72 h.p.i. in BEAS-2B cells, both intra- and extracellularly. In recent years, studies with recombinant viruses in three-dimensional cultures have described similar results, both in the CPE caused by the virus and in the replicative cycle (Geiser et al., 2021; Kinder et al., 2020). All these results show that our model of infection in the Vero-CCL cell line with this wild-type virus (A_2 hMPV), despite its isolation difficulties, is very efficient and representative of *in vivo* infection by hMPV.

One of the aims of this study was to evaluate the participation of the host cell actin cytoskeleton in hMPV replication. It is known that viruses such as PIV (Gupta et al., 1998), HIV (Sasaki et al., 2004) RSV (Kallewaard et al., 2005) and PIXV (Gil et al., 2017), amog others, take advantage of structures such as the cytoskeleton for entry, replication, morphogenesis and exit from the host cell. To this end, we used CytD, which binds to filamentous actin and disrupts its polymerization. Intracellularly, this drug not only prevented

bioRxiv preprint doi: https://doi.org/10.1101/2022.09.30.510364; this version posted October 1, 2022. The copyright holder for this preprint (which was not certified by peer review) is the author/funder, who has granted bioRxiv a license to display the preprint in perpetuity. It is made available under aCC-BY-NC-ND 4.0 International license.

the decrease in the percentage of hMPV-infected cells (during infection, 8 h.p.i. and 24 h.p.i.) but it also caused a significant increase in the number of fluorescent dots/infected cell, indicative of protein accumulations, in all treatments. These protein accumulations (fluorescent dots) coincide with the viral cytoplasmic structures called “inclusion bodies” (Derdowski et al., 2008; Najjar et al., 2016). According to Cifuentes-Muñoz (2017 and 2019), these represent the greatest sites of hMPV replication, specially at 24 h.p.i. In *Pneumovirus*, the formation of these structures is partially dependent on actin polymerization as reported by Kinder (2020). On the other hand, unlike Cifuentes (2017), our results show that an early treatment with CytD (8 h.p.i) also increases the extracellular viral production at this time, indicating that MFL interruption could facilitate the entry of viral particles into the host cell. This represents an increase in intracellular viral load and a decrease in virus release times, compared to the control growth curve. Notwithstanding, our results agree with Cifuentes regarding the decrease in extracellular viral load from 24 h.p.i., in this case in the treatment during the first 24 hours.

A series of studies suggest that hMPV is a cell-associated virus and that its efficient spread and successful infection could be related to cell-cell transmission (Kallewaard et al., 2005; Merwaiss et al., 2018; Mothes et al., 2010; Roberts et al., 2015). Actin disruption could be interrupting cell-cell transmission due to which the new virions would be looking for other routes to exit and accumulate in the extracellular environment. Therefore, actin dynamics is essential for hMPV infection since it allows the virus to spread between cells, regardless of the extracellular viral load (Najjar et al., 2016). This could explain the accumulation of viral proteins in the cell cytoplasm and the decrease of viral production in the extracellular environment after exposure to CytD for 24 h.p.i.

Since MFLs are involved in the transport of viral nucleocapsids and inclusion bodies to the assembly sites and in their subsequent release to the extracellular environment (Cifuentes-

bioRxiv preprint doi: https://doi.org/10.1101/2022.09.30.510364; this version posted October 1, 2022. The copyright holder for this preprint (which was not certified by peer review) is the author/funder, who has granted bioRxiv a license to display the preprint in perpetuity. It is made available under aCC-BY-NC-ND 4.0 International license.

muñoz et al., 2017; Cifuentes-Muñoz and Ellis Dutch, 2019), it is reasonable to think that short-term disruption of MFLs with CytD would facilitate internalization of viral particles into the cells. In contrast, long-term treatment with CytD (24 h.p.i), could prevent the transport of viral proteins and/or the nucleocapsid to the assembly sites, reducing the accumulation of cytoplasmic viral proteins and the extracellular viral production.

Despite the years since its discovery, the cell biology of hMPV infection remains poorly understood. This study broadens our knowledge on the isolation and growth curve characterization of a wild-type hMPV obtained from a clinical sample. Furthermore, the findings of this research provide new insights on hMPV infection as well as on the actin cytoskeleton role in viral replication, thus contributing to the understanding of hMPV internalization and spreading mechanisms.

MATERIALS AND METHODS

Cell culture and Virus isolation

Vero cells (Vero CCL- 81, ATCC® CCL-81) were grown in Minimum Essential Medium (MEM) (GIBCOBRL®) with 5-10% fetal bovine serum (FBS, Natocor), 1% antibiotic and antimycotic (Antibiotic Antimycotic Solution, Penicillin and Streptomycin 100X, Stabilized, GIBCO), at 37 °C and 5% CO_2.

Human Metapneumovirus was isolated from nasopharyngeal aspirates (NPA) of hospitalized young children in Cordoba, Argentina. All procedures were complied with the principles outlined by the Declaration of Helsinki and were approved by an Independent Ethics Committee of Hospital de Niños "Santísima Trinidad" (CIEIS) Protocol: 05/2011. The volunteers who offered samples, signed written assent/consent and their personal data was kept anonymous.

bioRxiv preprint doi: https://doi.org/10.1101/2022.09.30.510364; this version posted October 1, 2022. The copyright holder for this preprint (which was not certified by peer review) is the author/funder, who has granted bioRxiv a license to display the preprint in perpetuity. It is made available under aCC-BY-NC-ND 4.0 International license.

The infection protocol was adapted from Van den Hoogen (2001). As infection medium MEM with 0.00125% trypsin (Trypsin Solution 10X, SIGMA®) was used to allow F-protein cleavage, 0.3% bovine serum albumin (BSA) (Bovine Albumin, SIGMA®) and 1% antibiotic and antimycotic (Antibiotic Antimycotic Solution, Penicillin and Streptomycin 100X, Stabilized, GIBCO). The NPA positive was diluted in 2 ml of MEM without FBS and then centrifuged at 1500 r.p.m. for 5 minutes to clean the sample (NPA supernatant). The viral inoculum was prepared with 150 µl of NPA supernatant and 50 µl of infection MEM (200 µl: final volume). Vero cells monolayers (70-80% confluence) were grown in a 24-well plate with MEM (10% FBS and 1% ATB). Twenty-four hours later, the plate was washed three times with balanced saline buffer (PBS), 200 µl of the viral inoculum was added in each well and centrifuged at 2000 r.p.m. for 15 minutes (IEC International Refrigerated Centrifuge Model: PR-2). Afterwards, the plate was incubated at 37 °C and 5% CO_2 for 2 hours, the monolayers were washed three times with PBS and 1 ml of infection MEM per well was added. The infection MEM was changed at 4, 7, 10, 14, 17, and 21 days post-infection (d.p.i.) and the culture supernatants were stored until processed at -70 °C. Cell cultures were observed daily for cytopathic effect by phase contrast microscopy. Three blind passages for 21 days each were performed. The hMPV positive culture supernatants were then used as an infection inoculum for the following experiments.

RT-PCR

Viral nucleic acids were extracted with the QIAamp® Viral RNA Mini Kit (Qiagen, GmbH, Hilden, Germany) from 140 µl of culture supernatants collected following the manufacturer's instructions. RT-PCR for the detection of the hMPV N gene was used to amplify a 199 bp fragment, using the Qiagen OneStep RT-PCR kit (Qiagen, Hilden, Germany). The conventional RT-PCR was adapted from Bouscambert-Duchamp (Bouscambert-Duchamp et

bioRxiv preprint doi: https://doi.org/10.1101/2022.09.30.510364; this version posted October 1, 2022. The copyright holder for this preprint (which was not certified by peer review) is the author/funder, who has granted bioRxiv a license to display the preprint in perpetuity. It is made available under aCC-BY-NC-ND 4.0 International license.

al., 2005). We used the following hMPV primers: Fw 5´-GTGATGCACTCAAGAGATACCC-3´ and Rv 5´- CATTGTTTGACCGGCCCCATAA-3´, 50 µM each. Cycling conditions: 30 min at 50ºC and 15 min at 94ºC, followed by 40 cycles of 95ºC for 30 sec, 58ºC for 30 sec, and 72ºC for 1 min, plus one final step of 72ºC for 10 min. PCR products were separated by electrophoresis on a 1.5% agarose gel and visualized under UV light after ethidium bromide staining.

Indirect immunofluorescence assay

To visualize both the hMPV proteins and the actin network, we infected cells grown at 60% confluence on glass coverslips during 24 hours. At different times post-infection, cells were washed three times with PBS, fixed with 4% paraformaldehyde and 120 mM sucrose (Riedel-de Haën, Sigma-Aldrich Laborchemikalien GmbH, Seelze, Germany) for 20 min at room temperature and then washed with PBS, later they were permeabilized with 0.2% TritonTM X-100 (Sigma-Aldrich, St. Louis, MO) in PBS for 5 minutes at room temperature, washed three times with PBS and incubated with 5% bovine serum albumin (BSA, Sigma-Aldrich, St. Louis, MO) for one hour at room temperature. In order to detect viral proteins, cells were incubated overnight with the mouse anti-hMPV primary antibody (1/500) (IMAGEN™ hMPV. Oxoid Ltd.) in 1% BSA/PBS solution at 4 °C. Then the cells were washed three times with PBS and incubated with the goat anti-mouse secondary antibody Alexa Fluor 488 (1/1600) (Thermo Fisher Scientific Inc., Waltham, Massachusetts, USA) for 1 hour at room temperature. To visualize the actin filaments and nuclei, the fixed and permeabilized cells were labeled with Phalloidin-Tetramethyl rhodamine B (1/1000) (Sigma-Aldrich, St. Louis, MO) for 1 hour at room temperature and Hoesch (1X) for 5 minutes, respectively. Then, the monolayers were washed three times with PBS and the glass coverslips were mounted using Fluorsave (Calbiochem).

bioRxiv preprint doi: https://doi.org/10.1101/2022.09.30.510364; this version posted October 1, 2022. The copyright holder for this preprint (which was not certified by peer review) is the author/funder, who has granted bioRxiv a license to display the preprint in perpetuity. It is made available under aCC-BY-NC-ND 4.0 International license.

322

323 **Sequence and phylogenetic analysis**

324 The RT-PCR protocol was adaptaded from Van den Hoogen (Van Den Hoogen et al., 2004)
325 to amplify a 696 bp fragment of the F gene, using the Qiagen OneStep RT-PCR kit (Qiagen,
326 Hilden, Germany), with primers mix Fw 5´-CAATGCAGGTATAACACCAGCAATATC-3´
327 and Rv 5´-GCAACAATTGAACTGATCTTCAGGAAAC-3´ 50μM each. Cycling
328 conditions: 30 min at 42 °C and 8 min at 95 °C, followed by 40 cycles of 94 °C for 1 min, 40
329 °C for 2 min and 72 °C for 3 min, and a final step of 72 °C for 10 min. The amplified
330 products were separated by electrophoresis on a 1% agarose gel and visualized under UV
331 light after ethidium bromide staining.
332 The PCR product was purified with QIAquick Gel Extraction Kit (Qiagen, Hilden, Germany)
333 according to the manufacturer's instructions and subjected to direct nucleotide sequencing
334 reactions in both directions using the internal PCR primers by Macrogen, Inc. (Seoul, Korea).
335 The sequence obtained was edited with MEGA 4.0.2 (Tamura et al., 2007) and an alignment
336 was made with sequences available in the GenBank, using the ClustalW. The Maximum
337 Likelihood tree (ML) was constructed with the PhyML 3.0 software (Université de
338 Montpellier, Montpellier, France) (Guindon and Gascuel, 2003). The branch support was
339 evaluated via non-parametric bootstrapping with 1000 pseudoreplicates. The nucleotide
340 substitution model for the analyzed data set was selected according to the Akaike information
341 criteria implemented in the ModelTest 3.7 software (University 155 of Vigo, Galicia, Spain)
342 (Posada and Crandall, 1998). The F gene sequence was deposited in GenBank (accession no.
343 MN117139).

344

345 **Viral quantification by Sybr® RT-qPCR**

bioRxiv preprint doi: https://doi.org/10.1101/2022.09.30.510364; this version posted October 1, 2022. The copyright holder for this preprint (which was not certified by peer review) is the author/funder, who has granted bioRxiv a license to display the preprint in perpetuity. It is made available under aCC-BY-NC-ND 4.0 International license.

Viral RNA copies from supernatants obtained under different experimental conditions were determined by absolute quantification in an Applied Biosystems 7500 Fast Real-time PCR system. The manufacturer's protocol was adapted for the preparation of the reaction mix (AgPath-ID™ One-Step RT-PCR Reagents, Applied Biosystems™): 2X RT-PCR Buffer= 1X; Forward and reverse PCR primers= 50µM each; Syber Green (SYBR™ Green 10000X-Invitrogen S-7563) dilution 1/100= 5.0 and -5; 25X RT-PCR Enzyme Mix (ArrayScript™ Reverse Transcriptase and AmpliTaq Gold® DNA Polymerase)= 1X. The final reaction volume was 25 µl, using 2.5 µl of viral RNA. Cycling conditions: 50 °C for 30 min; 45 cycles of 94 °C for 2 min 95 °C for 10 sec, 60 °C for 30 sec and 72 °C for 30 sec and a final step of 72 °C for 10 min. Data were observed in real-time and analyzed with the Virtual Curve qPCR program from Applied Biosystems (Thermo Fisher Connect™). The viral load in each sample was calculated from a standard curve performed with serial dilutions (10-1 to 10-12) from an hMPV N protein synthetic oligonucleotide (199 bp) (Ultramer® DNA Oligo) of known concentration (6.0219X1013 copies of RNA/µl).

HMPV Replication Curve

Vero cells were grown at 60% confluence on glass coverslips (12 mm in 24-well plate) for 24 hours and then infected with isolated hMPV ($1.97x10^6$ copies of RNA/ µl). The culture supernatants were harvested and the monolayers were fixed at different times: 8, 16, 24, 48, 72, and 96 hpi. Viral RNA was extracted using the QIAamp Viral RNA Mini Kit (Qiagen, GmbH, Hilden, Germany) following the manufacturer´s instructions and used for the detection and quantification of hMPV by Sybr (SYBR™ Green 10000X, Invitrogen) RT-qPCR (AgPath -ID™ One-Step RT-PCR Reagents, Applied Biosystems™). The mean number of copies of extracellular viral RNA/µl of supernatant was then calculated (Applied biosystems. Thermo Fisher Connect™).

bioRxiv preprint doi: https://doi.org/10.1101/2022.09.30.510364; this version posted October 1, 2022. The copyright holder for this preprint (which was not certified by peer review) is the author/funder, who has granted bioRxiv a license to display the preprint in perpetuity. It is made available under aCC-BY-NC-ND 4.0 International license.

The cells were processed for IF, as described in previous sections, and the number of fluorescent dots per infected cell were calculated through the analysis of fluorescence images using the ImageJ Fiji software (ImageJ 1.50c NIH. USA).

Pharmacological treatment

Vero cells at 60% confluence cultured on glass coverslips were infected with hMPV according to the protocol described in the previous section. Infected cells treated with Cytochalasin D (CytD) [2.5μM] (Gil et al., 2017) or vehicle were analized at different times during the viral replication cycle. Cells were exposed to CytD or vehicle during the 2 infection hours, as well as throughout the first 8 h.p.i. (experimental period between 0-24 h.p.i.); during the first and the last 24 hours (48-72 h.p.i) in an experimental period between 0-72 h.p.i. In each case, the supernatant was removed, the cells were washed 3 times with PBS and the infection medium was added according to each treatment. Culture supernatants and harvested cells were processed for RNA extraction and viral quantification by RT-qPCR and indirect immunofluorescence, respectively.

Microscopy, processing and digital image analysis

Immunostained cells were visualized using a conventional inverted epi-fluorescence microscope (Olympus IX81, Olympus Corporation, Shinjuku, Tokyo). Images were taken with regular fluorescence microscopy whith a CCD camera (Orca 1000, Hamamatsu Corp., Middlesex, NJ). Images were also taken with an inverted confocal microscope FV1000 (Olympus). The collection and processing of data from the images were analyzed with the ImageJ Fiji software (ImageJ 1.50c Wayne Rasband. National Institutes of Health, USA).

bioRxiv preprint doi: https://doi.org/10.1101/2022.09.30.510364; this version posted October 1, 2022. The copyright holder for this preprint (which was not certified by peer review) is the author/funder, who has granted bioRxiv a license to display the preprint in perpetuity. It is made available under aCC-BY-NC-ND 4.0 International license.

Quantification of intracellular infection was carried out by the percentage of infected cells and the number of fluorescent dots/ infected cell. Images were processed with Adobe Photoshop CS6 (Version 13.0.1.).

Statistical analysis

Data are representative of at least four independent experiments, values are given as mean ± standard error of the mean (SEM). Statistical analysis was carried out using Student unpaired *t*-test, or one-way ANOVA test to enable specific group comparison. $p < 0.05$ was considered statistically significant. All data and tests were analyzed and performed using GraphPad Prism 5.0 (GraphPad Prism versión 5.00 for Windows, GraphPad).

ACKNOWLEDGEMENTS

We would like to thank Bernadette van den Hoogen for receiving PER in her laboratory and for advising on the viral isolation protocol; Guadalupe Carballal[†] and Cristina Videla for generously providing hMPV wild type positive control; Celia Frutos and Lucia Ghietto for technical assistance in Real Time RT-qPCR; Santiago Mirazo for generously providing polyclonal antibodies; Carlos Mas for technical assistance in confocal microscopy at the Centro de Micro y Nanoscopía de Córdoba, CEMINCO-CONICET-Universidad Nacional de Córdoba, Córdoba, Argentina. We particularly want to thank Miss Stella Ascheri for general technical assistance.

COMPETING INTERESTS

No competing interests declared

FUNDING

bioRxiv preprint doi: https://doi.org/10.1101/2022.09.30.510364; this version posted October 1, 2022. The copyright holder for this preprint (which was not certified by peer review) is the author/funder, who has granted bioRxiv a license to display the preprint in perpetuity. It is made available under aCC-BY-NC-ND 4.0 International license.

This work was supported by grants from Secretaria de Ciencia y Tecnología - Universidad Nacional de Córdoba (SECYT Cat B. Nº 30820130100350CB; Cat. B. Nº 30820150100037CB; SECYT-Consolidar-I Nº 336 20180100191CB; SECYT-Consolidar-C Nº 33620180100091CB; PRIMAR-TP Nº 32520170100046CB). Fundación A. J. Roemmers (2014-2016 and 2018-2020 to A.C and 2017-2019 to P.E.R). The funding sources had no involvement in the study design, data collection, analysis and interpretation, writing of the manuscript or in the decision to submit the article for publication.

DATA AVAILABILITY

The data that support the findings of this study are available from the corresponding author [gpaglini@immf.uncor.edu] upon reasonable request

REFERENCES

Abiko, C., Mizuta, K., Itagaki, T., Katsushima, N., Ito, S., Matsuzaki, Y., Okamoto, M., Nishimura, H., Aoki, Y., Murata, T., et al. (2007). Outbreak of human metapneumovirus detected by use of the Vero E6 cell line in isolates collected in Yamagata, Japan, in 2004 and 2005. *J. Clin. Microbiol.* **45**, 1912–1919.

Afonso, C. L., Gaya, K. A., Bányai, K., Yīmíng Bào, Basler, C. F., Bavari, S., Bejerman, N., Blasdell, K. R., Briand, F.-X., Briese, T., et al. (2016). TAXONOMY OF THE ORDER MONONEGAVIRALES: UPDATE 2016. *Arch Virol.* **161**, 2351–2360.

Arnott, A., Vong, S., Sek, M., Naughtin, M., Beauté, J., Rith, S., Guillard, B., Deubel, V. and Buchy, P. (2013). Genetic variability of human metapneumovirus amongst an all ages population in Cambodia between 2007 and 2009. *Infect. Genet. Evol.* **15**, 43–52.

Ballegeer, M. and Saelens, X. (2020). Cell-Mediated Responses to Human

bioRxiv preprint doi: https://doi.org/10.1101/2022.09.30.510364; this version posted October 1, 2022. The copyright holder for this preprint (which was not certified by peer review) is the author/funder, who has granted bioRxiv a license to display the preprint in perpetuity. It is made available under aCC-BY-NC-ND 4.0 International license.

Metapneumovirus Infection. *Viruses* **12**, 3–22.

Bernal, L. J., Velandia-Romero, M., Guevara, C. and Castellanos, J. E. (2019). Human Metapneumovirus: Laboratory Methods for Isolation, Propagation, and Plaque Titration. *Intervirology* **61**, 301–306.

Boivin, G., Abed, Y., Pelletier, G., Ruel, L., Moisan, D., Côté, S., Peret, T. C. T., Erdman, D. D. and Anderson, L. J. (2002). Virological Features and Clinical Manifestations Associated with Human Metapneumovirus: A New Paramyxovirus Responsible for Acute Respiratory Tract Infections in All Age Groups. *J. Infect. Dis.* **186**, 1330–1334.

Bouscambert-Duchamp, M., Lina, B., Trompette, A., Moret, H., Motte, J. and Andréoletti, L. (2005). Detection of human metapneumovirus RNA sequences in nasopharyngeal aspirates of young french children with acute bronchiolitis by real-time reverse transcriptase PCR and phylogenetic analysis. *J. Clin. Microbiol.* **43**, 1411–1414.

Chan, P. K. S., Tam, J. S., Lam, C., Chan, E., Wu, A., Li, C., Buckley, T. A., Ng, K., Joynt, G. M., Cheng, F. W. T., et al. (2003). Human Metapneumovirus Detection in Patients with Severe Acute Respiratory Syndrome. *Emerg. Infect. Dis.* **9**, 1058–1063.

Choe, P. G., Kang, C. K., Suh, H. J., Jung, J., Kang, E., Lee, S. Y., Song, K.-H., Kim, H. Bin, Kim, N. J., Park, W. B., et al. (2020). Antibody Responses to SARS-CoV-2 at 8 Weeks Postinfection in Asymptomatic Patients. *Emerg. Infect. Dis.* **26**,.

Cifuentes-muñoz, N., Branttie, J., Slaughter, K. B. and Dutch, R. E. (2017). Human Metapneumovirus Induces Transcription. *J. Virol.* **91**, 1–18.

Cifuentes-Muñoz, N. and Ellis Dutch, R. (2019). To assemble or not to assemble: The changing rules of pneumovirus transmission. *Virus Res.* **265**, 68–73.

bioRxiv preprint doi: https://doi.org/10.1101/2022.09.30.510364; this version posted October 1, 2022. The copyright holder for this preprint (which was not certified by peer review) is the author/funder, who has granted bioRxiv a license to display the preprint in perpetuity. It is made available under aCC-BY-NC-ND 4.0 International license.

463 **Cifuentes-Muñoz, N., Najjar, F. El and Dutch, R. E.** (2020). Viral cell-to-cell spread:
464 Conventional and non-conventional ways. In *Advances in Virus Research*, pp. 5985–125.

465 **Cox, R. G., Mainou, B. A., Johnson, M., Hastings, A. K., Schuster, J. E., Dermody, T. S.**
466 **and Williams, J. V.** (2015). Human Metapneumovirus Is Capable of Entering Cells by
467 Fusion with Endosomal Membranes. *PLoS Pathog.* **11**, 1–29.

468 **Deffrasnes, C., Côté, S. and Boivin, G.** (2005). Analysis of Replication Kinetics of the
469 Human Metapneumovirus in Different Cell Lines by Real-Time PCR. *J. Clin. Microbiol.*
470 **43**, 488–490.

471 **Derdowski, A., Peters, T. R., Glover, N., Qian, R., Utley, T. J., Burnett, A., Williams, J.**
472 **V., Spearman, P. and Crowe, J. E.** (2008). Human metapneumovirus nucleoprotein
473 and phosphoprotein interact and provide the minimal requirements for inclusion body
474 formation. *J. Gen. Virol.* **89**, 2698–2708.

475 **Galiano, M., Trento, A., Ver, L., Carballal, G. and Videla, C.** (2006). Genetic
476 Heterogeneity of G and F Protein Genes From Argentinean Human Metapneumovirus
477 Strains. *J. Med. Virol.* **78**, 631–637.

478 **Geiser, J., Boivin, G., Huang, S., Constant, S., Kaiser, L., Tapparel, C. and Essaidi-**
479 **Laziosi, M.** (2021). RSV and HMPV Infections in 3D Tissue Cultures: Mechanisms
480 Involved in Virus-Host and Virus-Virus Interactions. *Viruses* **13**, 1–15.

481 **Gil, P. I., Albrieu-Llinás, G., Mlewski, E. C., Monetti, M., Fozzatti, L., Cuffini, C.,**
482 **Fernández Romero, J., Kunda, P. and Paglini, M. G.** (2017). Pixuna virus modifies
483 host cell cytoskeleton to secure infection. *Sci. Rep.* **7**, 1–9.

484 **Guindon, S. and Gascuel, O.** (2003). A Simple, Fast, and Accurate Algorithm to Estimate
485 Large Phylogenies by Maximum Likelihood. *Syst. Biol.* **52**, 696–704.

bioRxiv preprint doi: https://doi.org/10.1101/2022.09.30.510364; this version posted October 1, 2022. The copyright holder for this preprint (which was not certified by peer review) is the author/funder, who has granted bioRxiv a license to display the preprint in perpetuity. It is made available under aCC-BY-NC-ND 4.0 International license.

Gupta, S., De, B. P., Drazba, J. A. and Banerjee, A. K. (1998). Involvement of actin microfilaments in the replication of human parainfluenza virus type 3. *J. Virol.* **72**, 2655–2662.

Jumat, M. R., Nguyen Huong, T., Wong, P., Loo, L. H., Tan, B. H., Fenwick, F., Toms, G. L. and Sugrue, R. J. (2014). Imaging analysis of human metapneumovirus-infected cells provides evidence for the involvement of F-actin and the raft-lipid microdomains in virus morphogenesis. *Virol. J.* **11**, 1–12.

Kallewaard, N. L., Bowen, A. L. and Crowe, J. E. (2005). Cooperativity of actin and microtubule elements during replication of respiratory syncytial virus. *Virology* **331**, 73–81.

Kim, C. K., Choi, J., Callaway, Z., Kim, H. Bin, Chung, J. Y., Koh, Y. Y. and Shin, B. M. (2010). Clinical and epidemiological comparison of human metapneumovirus and respiratory syncytial virus in Seoul, Korea, 2003-2008. *J. Korean Med. Sci.* **25**, 342–347.

Kinder, J. T., Moncman, C. L., Barrett, C., Jin, H., Kallewaard, N. and Dutch, R. E. (2020). Respiratory Syncytial Virus and Human Metapneumovirus Infections in Three-Dimensional Human Airway Tissues Expose an Interesting Dichotomy in Viral Replication, Spread, and Inhibition by Neutralizing Antibodies. *J. Virol.* **94**,.

Lee, H., Woo, H. M., Kim, K., Park, S., Park, M. S., Kim, S. S. and Kim, Y. J. (2019). Improving pneumovirus isolation using a centrifugation and AZD1480 combined method. *J. Microbiol. Biotechnol.* **29**, 2006–2013.

Loo, L. H., Jumat, M. R., Fu, Y., Ayi, T. C., Wong, P. S., Tee, N. W. S., Tan, B. H. and Sugrue, R. J. (2013). Evidence for the interaction of the human metapneumovirus G and F proteins during virus-like particle formation. *Virol. J.* **10**, 1–13.

bioRxiv preprint doi: https://doi.org/10.1101/2022.09.30.510364; this version posted October 1, 2022. The copyright holder for this preprint (which was not certified by peer review) is the author/funder, who has granted bioRxiv a license to display the preprint in perpetuity. It is made available under aCC-BY-NC-ND 4.0 International license.

509 **Mehedi, M., McCarty, T., Martin, S. E., Le Nouën, C., Buehler, E., Chen, Y. C.,**
510 **Smelkinson, M., Ganesan, S., Fischer, E. R., Brock, L. G., et al.** (2016). Actin-
511 Related Protein 2 (ARP2) and Virus-Induced Filopodia Facilitate Human Respiratory
512 Syncytial Virus Spread. *PLoS Pathog.* **12**, 1–35.

513 **Merwaiss, F., Czibener, C. and Alvarez, D. E.** (2018). Cell-to-cell transmission is the main
514 mechanism supporting bovine viral diarrhea virus spread in cell culture. *J. Virol.*

515 **Mothes, W., Sherer, N. M., Jin, J. and Zhong, P.** (2010). Virus Cell-to-Cell Transmission.
516 *J. Virol.* **84**, 8360–8368.

517 **Najjar, F. El, Cifuentes-Muñoz, N., Chen, J., Zhu, H., Buchholz, U. J., Moncman, C. L.**
518 **and Dutch, R. E.** (2016). Human metapneumovirus Induces Reorganization of the Actin
519 Cytoskeleton for Direct Cell-to-Cell Spread. *PLoS Pathog.* 1–30.

520 **Nao, N., Sato, K., Yamagishi, J., Tahara, M., Nakatsu, Y., Seki, F., Katoh, H., Ohnuma,**
521 **A., Shirogane, Y., Hayashi, M., et al.** (2019). Consensus and variations in cell line
522 specificity among human metapneumovirus strains. *PLoS One* **14**, 1–21.

523 **Nao, N., Saikusa, M., Sato, K., Sekizuka, T., Usuku, S., Tanaka, N., Nishimura, H. and**
524 **Takeda, M.** (2020). Recent molecular evolution of human metapneumovirus (HMPV):
525 Subdivision of HMPV a2b strains. *Microorganisms* **8**, 1–14.

526 **Posada, D. and Crandall, K. A.** (1998). MODELTEST: Testing the model of DNA
527 substitution. *Bioinformatics* **14**, 817–818.

528 **Reina, J., Ferres, F., Alcoceba, E., Mena, A., de Gopegui, E. R. and Figuerola, J.** (2007).
529 Comparison of different cell lines and incubation times in the isolation by the shell vial
530 culture of human metapneumovirus from pediatric respiratory samples. *J. Clin. Virol.* **40**,
531 46–49.

bioRxiv preprint doi: https://doi.org/10.1101/2022.09.30.510364; this version posted October 1, 2022. The copyright holder for this preprint (which was not certified by peer review) is the author/funder, who has granted bioRxiv a license to display the preprint in perpetuity. It is made available under aCC-BY-NC-ND 4.0 International license.

Roberts, K. L., Manicassamy, B. and Lamb, R. A. (2015). Influenza A Virus Uses Intercellular Connections To Spread to Neighboring Cells. *J. Virol.* **89**, 1537–1549.

Rodriguez, P. E., Frutos, M. C., Adamo, M. P., Cuffini, C., Cámara, J. A., Paglini, M. G., Moreno, L. and Cámara, A. (2020). Human Metapneumovirus: Epidemiology and genotype diversity in children and adult patients with respiratory infection in Córdoba, Argentina. *PLoS One* **15**, e0244093.

Sasaki, H., Ozaki, H., Karaki, H. and Nonomura, Y. (2004). Actin filaments play an essential role for transport of nascent HIV-1 proteins in host cells. *Biochem. Biophys. Res. Commun.* **316**, 588–593.

Sato, K., Watanabe, O., Ohmiya, S., Chiba, F., Suzuki, A., Okamoto, M., Younghuang, J., Hata, A., Nonaka, H., Kitaoka, S., et al. (2017). Efficient isolation of human metapneumovirus using MNT-1, a human malignant melanoma cell line with early and distinct cytopathic effects. *Microbiol. Immunol.* **61**, 497–506.

Schowalter, R. M., Smith, S. E. and Dutch, R. E. (2006). Characterization of Human Metapneumovirus F Protein-Promoted Membrane Fusion: Critical Roles for Proteolytic Processing and Low pH. *J. Virol.* **80**, 10931–10941.

Shafagati, N. and Williams, J. (2018). Human metapneumovirus - what we know now. *F1000Research* **7**, 1–11.

Shahriari, S., Gordon, J. and Ghildyal, R. (2016). Host cytoskeleton in respiratory syncytial virus assembly and budding. *Virol. J.* **13**, 1–11.

Shahriari, S., Wei, K. J. and Ghildyal, R. (2018). Respiratory syncytial virus matrix (M) protein interacts with actin in vitro and in cell culture. *Viruses* **10**, 7–12.

Tamura, K., Dudley, J., Nei, M. and Kumar, S. (2007). MEGA4: Molecular Evolutionary

bioRxiv preprint doi: https://doi.org/10.1101/2022.09.30.510364; this version posted October 1, 2022. The copyright holder for this preprint (which was not certified by peer review) is the author/funder, who has granted bioRxiv a license to display the preprint in perpetuity. It is made available under aCC-BY-NC-ND 4.0 International license.

555 Genetics Analysis (MEGA) software version 4.0. *Mol. Biol. Evol.* **24**, 1596–1599.

556 **Tollefson, S. J., Cox, R. G. and Williams, J. V** (2010). Studies of culture conditions and
557 environmental stability of human metapneumovirus. *Virus Res.* **151**, 54–59.

558 **Van Den Hoogen, B. G., De Jong, J. C., Groen, J., Kuiken, T., De Groot, R., Fouchier, R.**
559 **A. M. and Osterhaus, A. D. M. E.** (2001). A newly discovered human pneumovirus
560 isolated from young children with respiratory tract disease. *Nat. Med.* **7**, 719–724.

561 **Van Den Hoogen, B. G., Osterhaus, D. M. E. and Fouchier, R. A. M.** (2004). Clinical
562 impact and diagnosis of human metapneumovirus infection. *Pediatr. Infect. Dis. J.* **23**,
563 25–32.

564 **Velez Rueda, A. J., Mistchenko, A. S. and Viegas, M.** (2013). Phylogenetic and
565 Phylodynamic Analyses of Human Metapneumovirus in Buenos Aires (Argentina) for a
566 Three-Year Period (2009-2011). *PLoS One* **8**, 1–10.

567 **Vicente, D., Montes, M., Cilla, G., Perez-Yarza, E. G. and Perez-Trallero, E.** (2006).
568 Differences in clinical severity between genotype A and genotype B human
569 metapneumovirus infection in children. *Clin. Infect. Dis.* **42**, 111–113.

570 **Williams, J. V, Tollefson, S. J., Johnson, J. E., Jr, J. E. C. and Crowe, J. E.** (2005). The
571 Cotton Rat (Sigmodon hispidus) Is a Permissive Small Animal Model of Human
572 Metapneumovirus Infection , Pathogenesis , and Protective Immunity The Cotton Rat (
573 Sigmodon hispidus) Is a Permissive Small Animal Model of Human Metapneumovirus
574 Infection. *J. Virol.* **79**, 10944–10951.

575 **Yang, H., He, H., Tan, B., Liu, E., Zhao, X. and Zhao, Y.** (2016). Human
576 metapneumovirus uses endocytosis pathway for host cell entry. *Mol. Cell. Probes* **30**,
577 231–237.

bioRxiv preprint doi: https://doi.org/10.1101/2022.09.30.510364; this version posted October 1, 2022. The copyright holder for this preprint (which was not certified by peer review) is the author/funder, who has granted bioRxiv a license to display the preprint in perpetuity. It is made available under aCC-BY-NC-ND 4.0 International license.

578 **Zhang, Y., Wei, Y., Li, J. and Li, J.** (2012a). Development and optimization of a direct
579 plaque assay for human and avian metapneumoviruses. *J. Virol.* **185**, 61–68.

580 **Zhang, C., Du, L. N., Zhang, Z. Y., Qin, X., Yang, X., Liu, P., Chen, X., Zhao, Y., Liu, E.**
581 **M. and Zhao, X. D.** (2012b). Detection and genetic diversity of human
582 metapneumovirus in hospitalized children with acute respiratory infections in Southwest
583 China. *J. Clin. Microbiol.* **50**, 2714–2719.

584 **Zhou, Z., Zhang, P., Cui, Y., Zhang, Y., Qin, X., Li, R., Liu, P., Dou, Y., Wang, L. and**
585 **Zhao, Y.** (2020). Experiments Investigating the Competitive Growth Advantage of Two
586 Different Genotypes of Human Metapneumovirus: Implications for the Alternation of
587 Genotype Prevalence. *Sci. Rep.* **10**, 1–11.

588

589

bioRxiv preprint doi: https://doi.org/10.1101/2022.09.30.510364; this version posted October 1, 2022. The copyright holder for this preprint (which was not certified by peer review) is the author/funder, who has granted bioRxiv a license to display the preprint in perpetuity. It is made available under aCC-BY-NC-ND 4.0 International license.

FIGURE LEGENDS

Fige. 1. Human Metapneumovirus (hMPV) isolation and identification. A and B: Representative images of uninfected and infected VERO cells with hMPV. **A-** Images were obtained with phase contrast microscopy at low magnification, showing the viral infection cytopathic effect (CPE), which is visible at 14 d.p.i as cell rounding and shedding. Uninfected cells (top panel) and infected cells (bottom panel) at 4, 7 and 14 days d.p.i. **B-** The location of the hMPV protein through indirect immunofluorescence (see Materials and Methods), hMPV F protein (green), MFLs (red) and nuclei (blue) are shown. A temporary sequence of 4 to 14 days in non infected (top panel) and infected cells (bottom panel). **C-** Amplification products (RT-PCR) of the hMPV N protein region (199 bp) by agarose gel electrophoresis. Bands corresponding to culture supernatants of infected cells collected at 4, 7 and 14 d.p.i. and positive controls (C+) are shown. Uninfected cells collected at the same times are included (C-). MPM: molecular weight marker. **D-** Images obtained with confocal microscopy, showing that the hMPV F protein accumulates near the nucleus at 48 h.p.i. **E-** Confocal microscopy images where viral proteins are observed at 0 and 96 h.p.i.. The bottom panel shows a transverse optical section where the viral label is evidenced in the cell cytoplasm decorating the MFLs. **F-** A maximum-likelihood tree (PhyML software) was constructed, using the GTR+G model with parameters suggested by JModelTest 3.7 with bootstraps and 1000 pseudoreplicates. A1: strains to hMPV subgroup A1. A2: strains to hMPV subgroup A2. B1: strains to hMPV subgroup B1. B2: strains to hMPV subgroup B2. Avian MPV (aMPV) was used to root the tree. The strain of interest is marked in bold. The scale bar indicates the changes between nucleotides. Scale bar: 20 µm.

Fig. 2. HMPV viral replication curve. A- Quantification of intracellular and extracellular viral production through the cytoplasmic viral F protein (bars, left axis) and the number of copies of viral RNA in the extracellular medium (curve, right axis). Quantification was performed at 8, 16, 24, 48, 72 and 96 h.p.i. **B-** Percentage of quantified infected cells was determined by the number of cells with or without fluorescent dots at 0, 8, 24, 48, and 72 h.p.i. **C-** Representative images of the temporal sequence of infection (0-96 h.p.i.). The hMPV F protein label (green) and nuclei (Hoesch-Blue) are

bioRxiv preprint doi: https://doi.org/10.1101/2022.09.30.510364; this version posted October 1, 2022. The copyright holder for this preprint (which was not certified by peer review) is the author/funder, who has granted bioRxiv a license to display the preprint in perpetuity. It is made available under aCC-BY-NC-ND 4.0 International license.

617 observed. Scale bar: 20 μm. Results are the mean ± SEM (one-way ANOVA with Tukey test post hoc
618 test). *** p <0.0001 ** p <0.001 * p <0.01.

619

620 **Fig. 3. Effect of disruption of Actin Microfilaments (MFLs) with CytD. A-** Images of CytD
621 treatments in hMPV infected cells at different times of the growth curve: CytD during infection (2 h),
622 8 h.p.i. and 24 h.p.i. Immunofluorescence performed with specific hMPV antibodies anti-protein F
623 (green), MFLs (Phalloidin-Rho, red) and nuclei (Hoesch, blue). **B-** Percentage of infected cells after
624 CytD treatment in relation to vehicle control. CytD treatment during infection (2 h): a significant
625 increase was observed at 24 h.p.i. (0 h p= 0.6544; 24 h.p.i. p< 0.0001). CytD treatment during the first
626 8 h.p.i.: a significant increase was observed at 24 h.p.i. (8 h.p.i. p= 0.0773; 24 h.p.i. p<0.0001). In
627 CytD treatment during first 24 h.p.i. a significant increase was observed both at 24 and 72 h.p.i. (24
628 h.p.i p<0.0001; 72 h.p.i. p<0.0001). **C-** Number of fluorescent dots per infected cell in CytD treatment
629 and in controls. CytD treatment during infection (2 h): a significant increase was observed at 24 h.p.i.
630 (0 h p= 0.9816; 24 h.p.i. p< 0.0001). CytD treatment during the first 8 h.p.i.: a significant increase was
631 observed both at 8 and 24 h.p.i. (8 h.p.i p< 0.0001; 24 h.p.i. p< 0.0001). CytD treatment during the
632 first 24 h.p.i.: a significant increase was observed at 72 h.p.i. (24 h.p.i. p= 0.3886; 72 h.p.i. p<0.0001).
633 **D-** Quantification of extracellular viral RNA. CytD treatment during infection (2 h): a significant
634 increase in RNA copies was observed at 24 h.p.i. (p<0.0001). CytD treatment during the first 8 h.p.i.
635 caused a significant increase at 8 h.p.i. (p<0.0001). CytD treatment during the first 24 h.p.i. caused a
636 significant decrease in extracellular viral RNA copies, remaining constant until 72 h.p.i. (p< 0.0001).
637 Scale bar: 20 μm. Results are the mean ± SEM. Student unpaired *t* test was performed (*** =
638 p<0.0001).

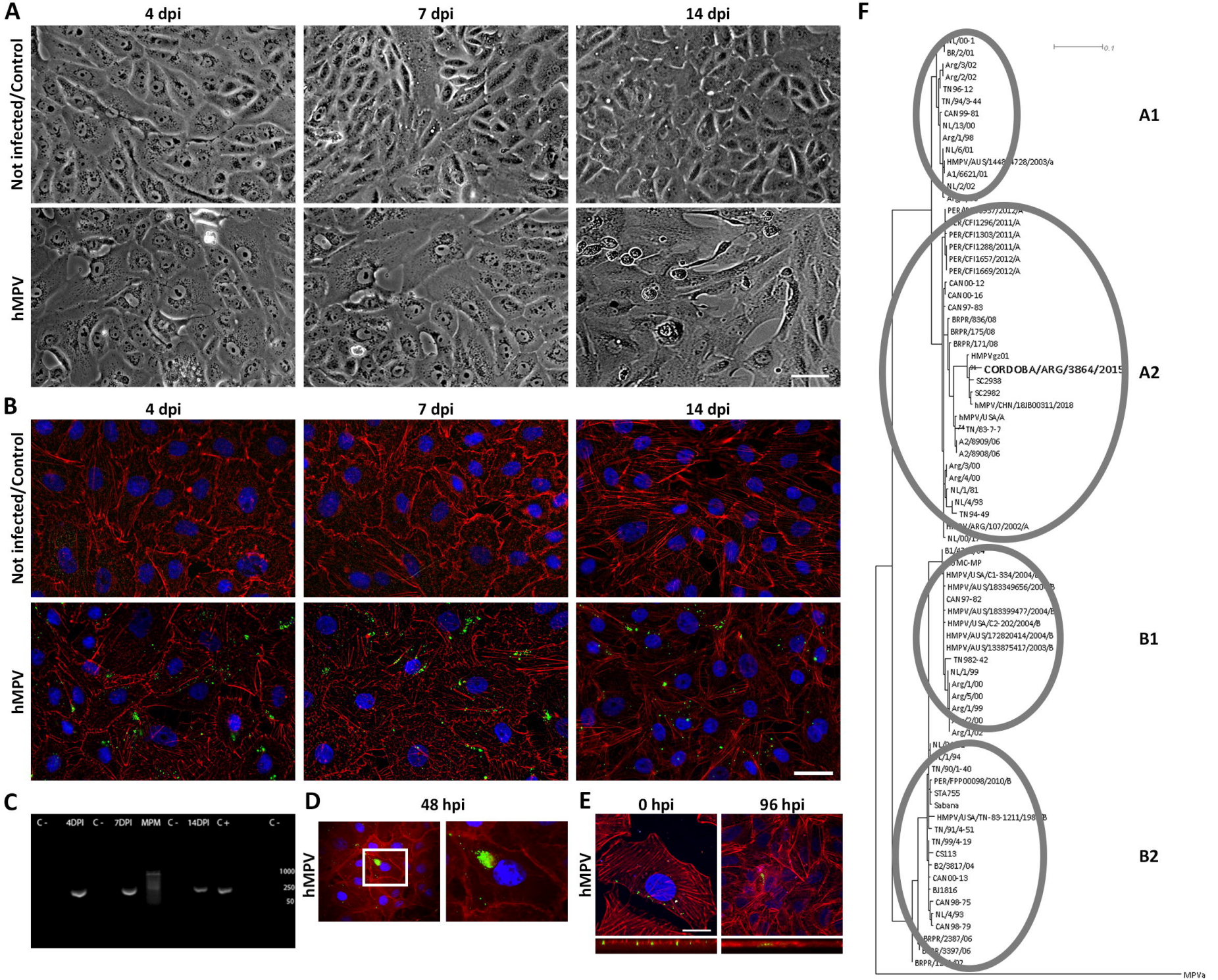
A
4 dpi
7 dpi
14 dpi
Not infected/Control
hMPV
B
4 dpi
7 dpi
14 dpi
Not infected/Control
hMPV
C
C -
4DPI
C -
7DPI
MPM
C -
14DPI
C +
C -
1000
250
50
D
48 hpi
hMPV
E
0 hpi
96 hpi
hMPV
F
A1
A2
B1
B2
CORDOBA/ARG/3864/2015
MPVa

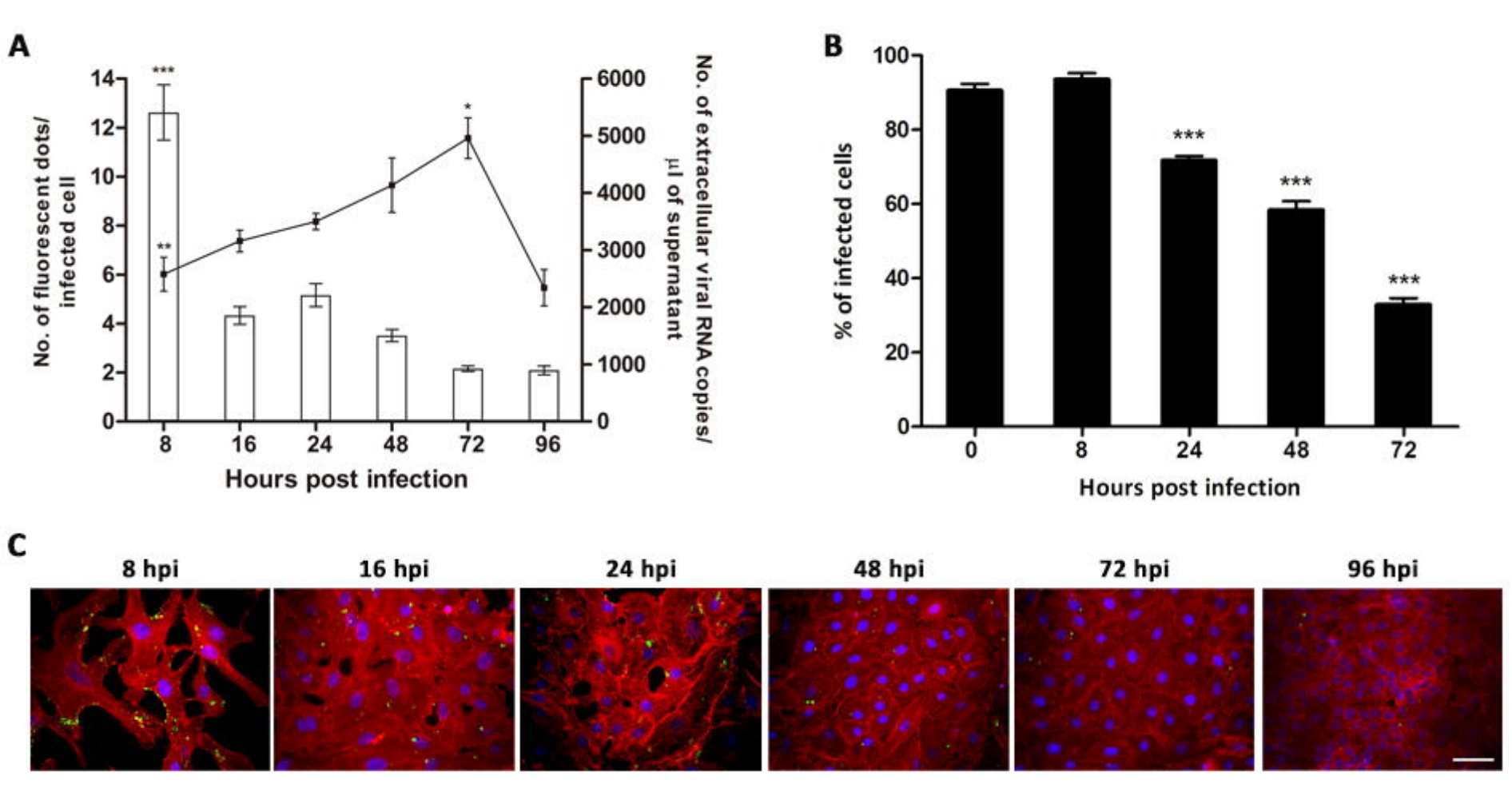
A
No. of fluorescent dots/ infected cell
No. of extracellular viral RNA copies/ µl of supernatant
Hours post infection
8
16
24
48
72
96
B
% of infected cells
Hours post infection
0
8
24
48
72
C
8 hpi
16 hpi
24 hpi
48 hpi
72 hpi
96 hpi

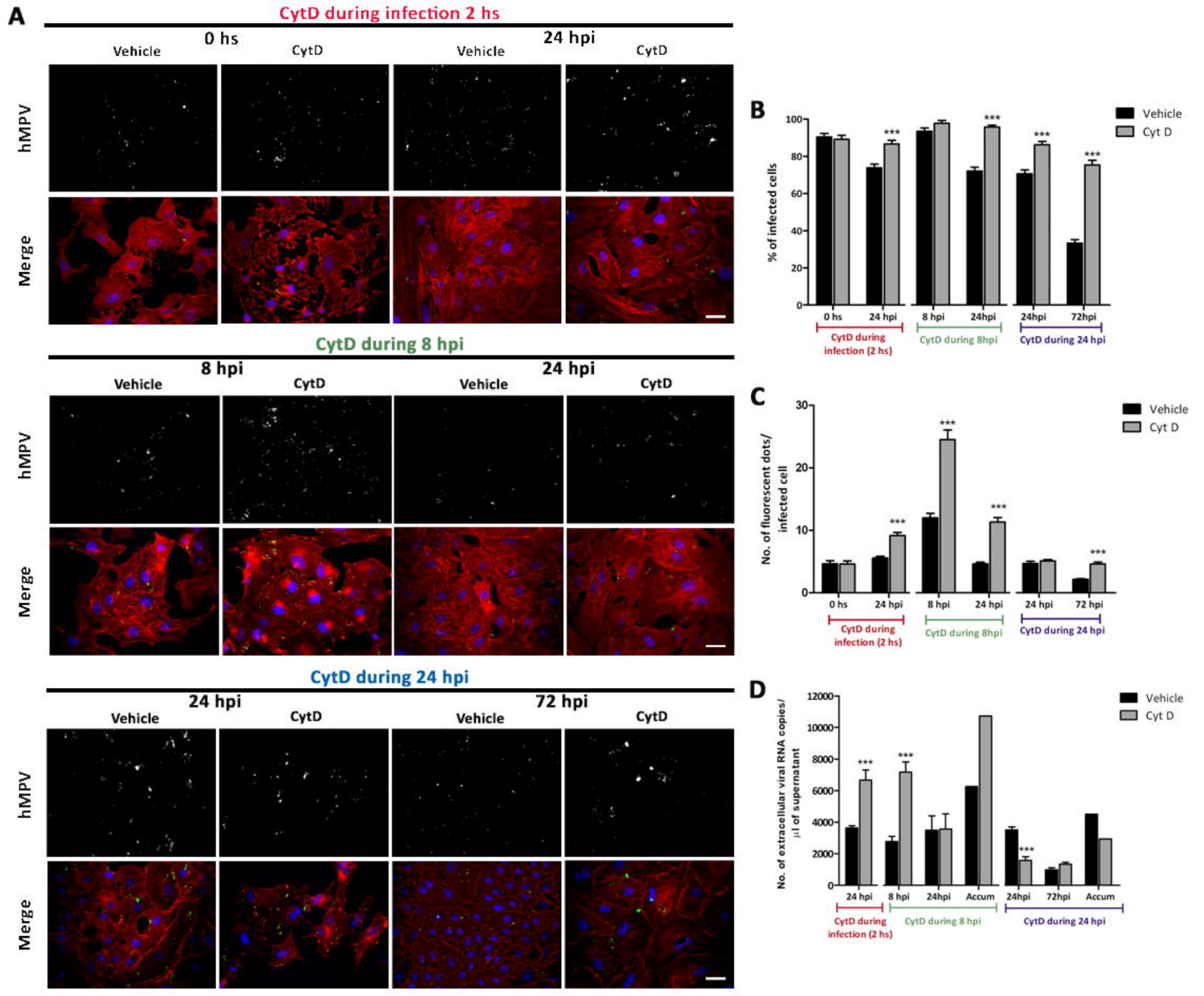
A
CytD during infection 2 hs
0 hs
24 hpi
Vehicle
CytD
Vehicle
CytD
hMPV
Merge
CytD during 8 hpi
8 hpi
24 hpi
Vehicle
CytD
Vehicle
CytD
hMPV
Merge
CytD during 24 hpi
24 hpi
72 hpi
Vehicle
CytD
Vehicle
CytD
hMPV
Merge
B
% of infected cells
Vehicle
Cyt D
0 hs
24 hpi
8 hpi
24hpi
24hpi
72hpi
CytD during infection (2 hs)
CytD during 8hpi
CytD during 24 hpi
C
No. of fluorescent dots/ infected cell
Vehicle
Cyt D
0 hs
24 hpi
8 hpi
24 hpi
24 hpi
72 hpi
CytD during infection (2 hs)
CytD during 8hpi
CytD during 24 hpi
D
No. of extracellular viral RNA copies/ µl of supernatant
Vehicle
Cyt D
24 hpi
8 hpi
24hpi
Accum
24hpi
72hpi
Accum
CytD during infection (2 hs)
CytD during 8 hpi
CytD during 24 hpi